A search for Star-Planet-Interactions in the υ Andromedae system at X-ray and optical wavelengths

K. Poppenhaeger[1], L. F. Lenz[2], A. Reiners[2], and J. H. M. M. Schmitt[1]

[1] Hamburger Sternwarte, Hamburg University, Gojenbergsweg 112, 21029 Hamburg, Germany
e-mail: `katja.poppenhaeger@hs.uni-hamburg.de`
[2] Universität Göttingen, Institut für Astrophysik, Friedrich-Hund-Platz 1, 37077 Göttingen, Germany

ABSTRACT

Context. Close-in, giant planets are expected to influence their host stars via tidal or magnetic interaction. But are these effects strong enough in suitable targets known so far to be observed with today's instrumentation?
Aims. The υ And system, an F8V star with a Hot Jupiter, was claimed to undergo cyclic changes in chromospheric activity indicators with its innermost planet's period. We want to investigate the stellar chromospheric and coronal activity over several months.
Methods. We therefore monitored the star in X-rays as well as at optical wavelengths to test coronal and chromospheric activity indicators for planet-induced variability, making use of the *Chandra* X-ray Observatory as well as the echelle spectrographs *FOCES* and *HRS* at Calar Alto (Spain) and the Hobby-Eberly Telescope (Texas, US), respectively.
Results. The stellar activity level is low, as seen both in X-rays as in Ca II line fluxes; the chromospheric data show variability with the stellar rotation period. We do not find activity variations in X-rays or in the optical which can be traced back to the planet.
Conclusions. Observational evidence for Star-Planet-Interactions in X-rays thus remains elusive.

Key words. Planet-star interactions – Stars: activity – Stars: coronae – Stars: chromospheres – X-rays: stars – Stars: individual: upsilon Andromedae – X-rays: individuals: upsilon Andromedae

1. Introduction

Interactions between stars and their giant planets have gained considerable attention during the last years. Since the discovery of 51 Peg b, a Jupiter-like planet in a four day orbit around a solar-like star, both the influence of stellar irradiation on planetary atmospheres has been investigated by various authors (cf. Lammer et al. 2003; Lecavelier Des Etangs 2007; Erkaev et al. 2007), as well as possible effects that giant planets may have on their host star's activity. Such Star-Planet-Interactions (SPI) are thought to happen via one of two major scenarios (Cuntz et al. 2000), tidal and magnetic interaction. In the tidal interaction process, the planet induces tidal bulges on the surface of the star which can cause enhanced stellar activity via increased turbulence in the photosphere. Magnetic interactions can increase stellar activity via magnetic reconnection of planetary and stellar magnetic field lines (Lanza 2008), or via Jupiter-Io-like interaction, i.e. flux tubes which connect star and planet and heat the stellar atmosphere at their footpoints (Goldreich & Lynden-Bell 1969; Schmitt 2009).

There have been dedicated searches for observational signatures of SPI in stellar chromospheres. Shkolnik et al. (2005) investigated 13 stars and found for two stars variations in the Ca II K line core fluxes, a common chromospheric activity indicator, which seemed to be in phase with the planetary orbit. The fact that flux excesses appeared once per orbit and not twice suggests that magnetic and not tidal interaction might have been at work. However, a follow-up study (Shkolnik et al. 2008) found only indications for variability with the stellar rotation period.

Other studies extended the search for SPI signatures into the X-ray regime to test for coronal activity changes in addition to the chromospheric hints found before. A statistical study by

Kashyap et al. (2008) claimed that stars with close-in planets are over-active by a factor of four in X-rays, but these authors had to use a large number of upper limits. Poppenhaeger et al. (2010) investigated a complete sample of all planet-bearing stars within 30 pc distance and found no correlation between stellar activity and planetary distance or mass which could not be traced back to selection effects. Scharf (2010) investigated a smaller sample of planet-hosting stars at distances of up to 60 pc and found indications for a lower floor of X-ray luminosity of stars with very close planets depending on the planetary mass; however, selection effects could not be ruled out for the low-mass planets in the sample.

This work investigates the υ And (HD 9826) system, one of the star-planet systems with hints for SPI signatures as published in Shkolnik et al. (2005), for such signatures in chromospheric as well as coronal data. υ And is an F8 star, orbited by a massive planet ($0.69 M_J$) in a 4.6 d ($a = 0.059$ AU) orbit, as well as by two other planets at much larger distances. This makes υ And a very suitable candidate to search for SPI signatures.

To look for signatures of Star-Planet-Interactions, we observed the υ And system for the first time nearly simultaneously at optical and X-ray wavelengths, thus testing for chromospheric as well as coronal variability.

2. Observations and data analysis

Our optical data were obtained with the FOCES echelle spectrograph at Calar Alto, Spain and with HRS, the echelle spectrograph mounted at HET in Texas, US. The X-ray data were collected with the Chandra X-ray Observatory. A complete list of our observations is given in Table 1.
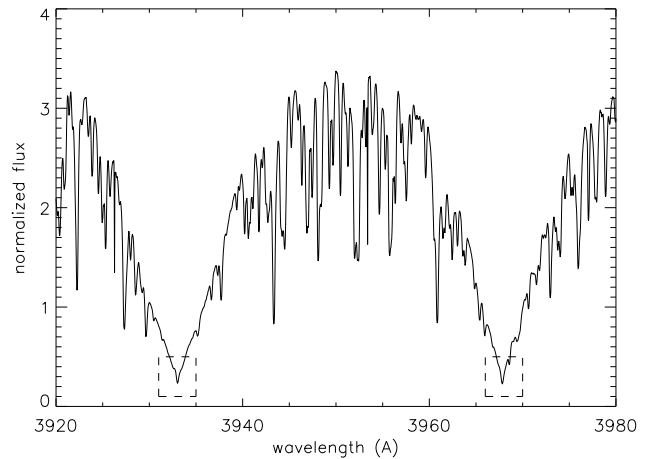
Table 1. Optical and X-ray observations of υ And. Integrated Ca II K line residuals are given for optical data, but the absolute scales of FOCES and HRS data are not comparable (see text); expected SPI state according to Shkolnik et al. (2005) given for X-ray data.

Instrument	MJD	Ca II K residual	exp. SPI state
FOCES (15μ)	55014.12	-0.05 ± 0.14	-
FOCES (15μ)	55015.12	-0.03 ± 0.19	-
FOCES (15μ)	55016.12	-0.05 ± 0.11	-
FOCES (15μ)	55017.12	-0.01 ± 0.11	-
FOCES (15μ)	55018.12	0.10 ± 0.14	-
FOCES (15μ)	55020.13	0.36 ± 0.14	-
FOCES (15μ)	55021.13	0.07 ± 0.11	-
FOCES (15μ)	55022.13	-0.03 ± 0.13	-
FOCES (15μ)	55023.13	-0.39 ± 0.20	-
FOCES (15μ)	55024.14	-0.24 ± 0.14	-
FOCES (15μ)	55025.13	-0.13 ± 0.14	-
FOCES (15μ)	55027.13	0.36 ± 0.09	-
FOCES (15μ)	55028.13	0.37 ± 0.09	-
FOCES (15μ)	55029.12	0.27 ± 0.14	-
FOCES (24μ)	55096.19	0.03 ± 0.17	-
FOCES (24μ)	55099.20	-0.08 ± 0.13	-
FOCES (24μ)	55100.20	-0.05 ± 0.17	-
FOCES (24μ)	55105.21	-0.02 ± 0.14	-
FOCES (24μ)	55107.20	-0.01 ± 0.18	-
FOCES (24μ)	55108.17	-0.01 ± 0.16	-
FOCES (24μ)	55109.17	-0.08 ± 0.16	-
FOCES (24μ)	55110.19	-0.17 ± 0.16	-
FOCES (24μ)	55169.00	0.13 ± 0.20	-
HET / HRS	55049.37	0.50 ± 0.21	-
HET / HRS	55083.27	-0.05 ± 0.16	-
HET / HRS	55090.25	-0.76 ± 0.20	-
HET / HRS	55110.44	-1.10 ± 0.20	-
HET / HRS	55135.12	-0.22 ± 0.14	-
HET / HRS	55139.34	-0.43 ± 0.16	-
HET / HRS	55141.33	0.72 ± 0.14	-
HET / HRS	55142.35	1.00 ± 0.16	-
HET / HRS	55146.33	0.35 ± 0.15	-
Chandra ACIS-S	55124.72	-	maximum
Chandra ACIS-S	55126.56	-	minimum
Chandra ACIS-S	55131.29	-	minimum
Chandra ACIS-S	55133.50	-	maximum

Fig. 1. Typical spectrum of υ And recorded with FOCES. The reversals in the Ca II H and K line cores (dashed boxes) are weak.

the possibility to study RV shifts, but does not interfere with our analysis of flux excesses in the Ca II H and K line cores.

A typical spectrum of the Ca II H and K lines of υ And is shown in Fig. 1. The reversals in the two line cores are weak, but clearly visible. The signal-to-noise ratio (S/N) of the final spectra is at ≈ 150 pixel^{-1} in the quasi-continuum between the H and K line and at ≈ 40 pixel^{-1} in the line cores, summing up to $S/N \approx 150$ in the complete line cores which stretch over ca. 15 pixels each.

The spectra were normalized by setting the flux of one template spectrum at 3929.5 Å to unity, giving a comparable normalization as the one used by Shkolnik et al. (2005). The remaining spectra were normalized by minimizing the scatter of the flux in two areas to the left and right of the Ca II K line reversal, specifically in the 3930-3932Å and 3934-3936Å range. Later on, a mean spectrum was subtracted from the individual spectra to determine the flux variations in the line cores (see section 3.1). We tested that shifting the normalization areas by 1-2Å outwards from the line cores does not significantly change our results. To further test if our normalization method might introduce false variability signals, we also applied our procedure to the Al I line near 3944Å, a photospheric line that should show no activity-related variations. In that part of the spectra, the multitude of lines present makes the normalization less exact, causing a higher overall scatter between the normalized spectra. However, the magnitude of the residuals of the individual spectra compared to the mean spectrum does not change near the Al I line although it has a comparable depth to the Ca II lines, indicating that the method itself does not produce false variability signals between the two normalization areas.

For subsequent analysis, the residuals at the Ca II K line core were integrated over a central range of 1Å. The corresponding error bars were calculated by estimating the statistical error in each bin to be the standard deviation of the residuals in the normalization ranges, and then calculating the 2σ error in the integrated area under the Ca II K line center by Monte-Carlo simulations.

2.1. Optical data from FOCES

We obtained 23 spectra of υ And with the FOCES echelle spectrograph installed at the 2.2m telescope at Calar Alto from July to December 2009. The 14 spectra obtained during July were recorded with the LOR#11i detector with 15μm pixel size, the other 9 spectra were recorded with the Site#1d detector with 24μm pixel size, all with an exposure time of 900s. The covered wavelength range was 3900–9500 Å.

The data were reduced with Calar Alto's standard echelle extraction routine d2.pro written in IDL (available from the Calar Alto data server ftp.caha.es). Mean dark frames were subtracted from the nightly spectra, which were then normalized using mean flat fields taken prior to the observations. Wavelength calibration was done with Thorium-Argon frames taken during the same night. The spectral resolution as inferred from the FWHM of ThAr lines is $R \sim 30000$. Since not all of our spectra have ThAr frames taken directly before or after the observation, we cross-correlated the spectra around the Ca II H and K lines and shifted the wavelength axis correspondingly. This deprives us of

2.2. Optical data from HRS

Nine spectra were taken with the HRS instrument at the HET with a resolution of $R \sim 60000$. The data reduction was similar

to the FOCES data reduction except for the use of flatfields. The HRS flatfields are taken with a separate, wider calibration fiber to allow 2D-flatfielding. However, the orders of the calibration fiber overlap in the Ca ɪɪ K region of the flatfields and thus cannot be used. We tested using standard star data as a surrogate for a flatfield but this added a lot of noise because of their relatively low data quality. To preserve the high signal-to-noise ratio of the spectra (S/N $\approx$ 90 near the Ca ɪɪ K core) we reduced the data without flatfielding.

A consequence of the lacking flatfields is that a direct comparison between the data from FOCES and HRS is not possible. We experimented with artificial, polynomial fits to the continua to obtain comparable line shapes in the Ca ɪɪ K line but did not achieve an acceptable solution. Thus, analyzing the residuals of the HRS data is possible, but normalization that allows direct comparison between the results from HRS and FOCES data cannot be performed. As a result the two data sets had to be analyzed individually.

The HRS spectra were normalized by first setting their flux at 3929.5 Å to unity. Then a reference spectrum was chosen and a polynomial was fitted to the quotient of each spectrum and the reference spectrum which represents the missing flatfield. The Ca ɪɪ K line was omitted from the fitting to avoid removing any variability in the line core. Each spectrum was divided by its fit to receive the normalized spectra.

2.3. X-ray data

We observed the υ And system with the *Chandra* X-ray telescope in four pointings of 15 ks ($\approx$ 4 h) each. These observations were scheduled such that two of them cover the expected maximum and two the expected minimum SPI-activity times, as inferred from optical observations done by Shkolnik et al. (2005) (see Table 1).

The data were reduced using standard procedures of the CIAO v.4.2 software package. υ And emits soft X-ray radiation with practically all photons having energies below 2 keV, its mean X-ray count rate is $\approx$ 0.025 cts/s in the 0.4-2 keV energy band. We produced light curves with 1 ks binning to obtain acceptable error bars as well as enough time resolution to identify possible flares. For the spectra, we used energy bins with at least 15 counts per bin for decent statistics. The spectral fitting was performed with Xspec v12.5.

Since υ And is an optically rather bright star (m_V = 4.09), the data were collected with a reduced frame time of 0.74s. Additionally, we only use data at energies above 400 eV to exclude possible optical contaminations at the low-energy sensitivity end of the detector.

3. Results

3.1. Chromospheric activity

Following Shkolnik et al. (2005), we computed separate median spectra for the FOCES and the HRS data and computed the residual fluxes of each spectrum compared to the respective median spectrum by subtracting the median spectra binwise from the individual spectra. We also computed the variation measured in standard deviations by dividing the residuals by the poissonian flux error of each bin of the individual spectra, neglecting the error in the median spectra. The results for the 15μ data, smoothed by 15 bins ($\approx$ 0.45Å), are shown in Fig. 2. For the 15μ data, which was recorded in July 2009 under very favorable weather conditions, we find variations in the Ca ɪɪ K line core at
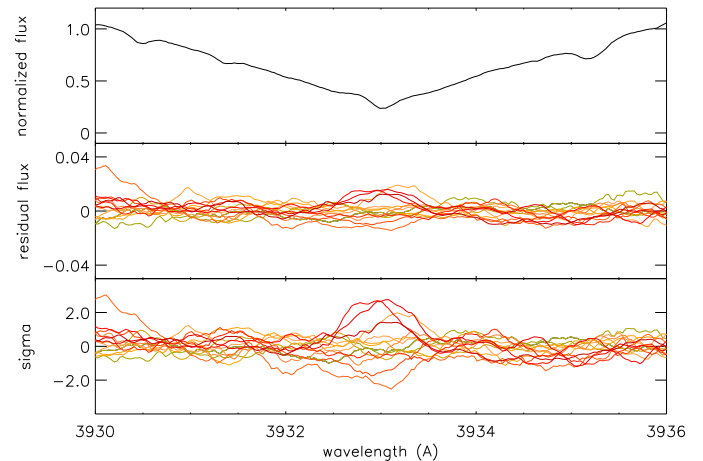
Fig. 2. Variability in Ca ɪɪ K line cores of the FOCES 15μ data. *upper panel:* normalized mean spectrum; *middle panel:* residual flux in the same normalization; *lower panel:* flux variation in standard deviations
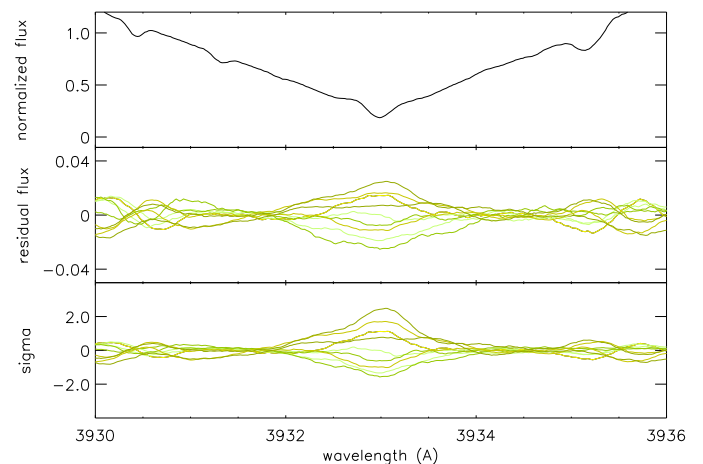
Fig. 3. Same as Fig. 2, but for HRS data.

$\approx 2\sigma$ levels; the HRS data shows similar variation (Fig. 3), while for the 24μ data, the overall noise level is so high that no additional variability in the line core can be identified by naked-eye inspection. Measured in relative flux deviations, the K line core flux varies at a $\pm$0.02 level in our chosen normalization, with an overall noise level of $\pm$0.01. Shkolnik et al. (2005) found for υ And a variation at a $\pm$0.01 level and an overall noise level of $\pm$0.002. Our noise level is much higher with $\pm$0.01, and so we interpret our $\pm$0.02 variation in the core to be not inconsistent with the previously found level of $\pm$0.01.

The Ca ɪɪ K line core fits into an interval of $\approx$ 1Å width, see for example Hall et al. (2007) and our data in Fig. 2. We therefore integrate the K line residuals from 3932.5-3933.5Å to obtain a measure for the total variation per spectrum. The crucial question now is whether there is a periodicity in this signal and which period can be associated with it.

The timeseries of our integrated residuals is shown in Fig. 4. The FOCES 15μ data show already by naked-eye inspection a variability which tracks a bit more than one cycle of a presumably sinusoidal variation with a periodicity of about eight to nine days. As discussed in section 2.2, the spectra from FOCES and

HET cannot be absolutely calibrated with respect to each other, and therefore also the calculated residuals are not comparable on an absolute scale. Thus we proceeded as follows: First, we calculated a Lomb-Scargle periodogram (Lomb 1976; Scargle 1982) of the collected optical data from FOCES, weighting the data points with their respective errors (see Gilliland & Baliunas 1987). This yields three significant peaks with false alarm probabilities (FAP) below 5%, corresponding to periods of $P = 9.3$ d, 8.7 d, and 8.2 d, sorted by descending significance. Then, we calculated a weighted Lomb-Scargle periodogram for the HRS data alone. This yields no significant periods with FAP below 20%, which is not too surprising since there are only nine data points from HRS, distributed over more than three months. Finally, we try to combine the HRS and FOCES residuals *ad hoc* by scaling down the HRS residuals by a factor of 0.4 so that the highest and lowest values match approximately in both datasets. This is a crude approximation at best; in the Lomb-Scargle periodogram, a possibly wrong scaling will lead to incorrect FAPs, but prominent peaks should still be reproduced reliably. The result is shown in Fig. 5. The periodogram of the combined data exhibits the strongest peak at $P = 9.5$ d with a nominal FAP of 9.8% (keeping in mind that the FAPs may be unreliable for the combined data set). The important point here is that we see a single, isolated main peak at a period which is also found in the FOCES data alone. In contrast to this, near the planetary orbital period of 4.6 d, or half its value, no significant peak appears in any of the periodograms.

If one chooses to interpret these findings as signatures of periodic activity variations, they are probably associated with the stellar rotation period. The star's rotational velocity $v \sin i$ was measured to be 9.5 ± 0.4 km/s by Gonzalez et al. (2010), its radius is computed by Henry et al. (2000) from stellar parameters as $1.6 R_\odot$, yielding a rotation period of ≈ 8.5 d, with rather large, but difficult to quantify errors, since the stellar radius was not determined observationally. Still, this stellar rotation period fits the possible periodic signal in our data better than the orbital period of the Hot Jupiter of 4.6 d. Additionally, we have a subset of our data consisting of nightly measurements in July 2010 which closely tracks one complete sinusoidal variation of ≈ 9 d period, making it rather unlikely that we see an alias of the planetary period here, but not the period of 4.6 d itself. This suggests that we see typical low-level stellar activity variations with the stellar rotation period which are not induced by Star-Planet-Interactions.

3.2. Coronal activity

We extracted X-ray lightcurves of υ And with 1 ks binning in the 0.4-2.0 keV energy band. The lightcurves (see Fig. 6) show variability at 50% level, but no large flares. The mean count rate is constant in observations 1,2 and 4; the third observation's mean count rate is somewhat lower by 25%.

A typical X-ray spectrum of υ And is shown in Fig. 7; these spectra have a total amount of ≈ 450 source counts, binned by 15 counts as a minimum to allow χ^2 statistics. The spectra of all four pointings cannot be fitted satisfactorily with thermal plasma models with solar abundances and one or two temperature components, while a one-temperature model with variable elemental abundances yields acceptable fits. The results of the spectral fitting performed in Xspec v.12.5 are given in Table 2; the abundances are relative to Grevesse & Sauval (1998). The modeled elemental abundances are interdependent with the derived emission measure and different combinations of both parameters lead to very similar results. For example, the best fits of the first and last observation give lower abundances and higher emission
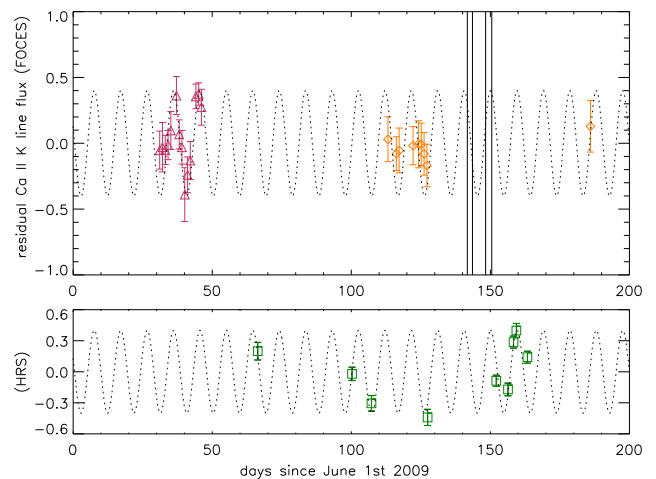
Fig. 4. Time series of Ca II residuals with highest probability period (9.5 d) indicated by the dotted line; red triangles and orange diamonds are 15μ and 24μ data from FOCES, green boxes are scaled-down HRS data with the same periodicity indicated. *Chandra* observation dates are indicated by vertical solid lines.
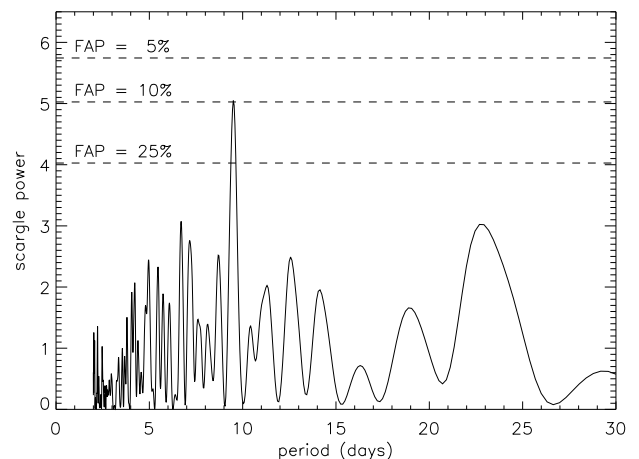
Fig. 5. Lomb-Scargle periodogram of Ca II K line residuals (weighted by their respective errors) with nominal false alarm probabilities given by the horizontal lines (see text).

measures than the fits of the other two pointings, but fixing the abundances to the values of the other observations yields comparable emission measures and almost the same fit quality.

Within errors, the spectral properties of all four observations are similar. The plasma temperature is rather low with ≈ 3 MK. The elemental abundances show a FIP effect, since elements with high first ionization potentials such as oxygen and neon are underabundant compared to iron with a low FIP. This is typical for stars with low to moderate coronal activity, determined by the activity indicator $\log L_X/L_{bol} < -4$. υ And's mean X-ray luminosity in these observations is 27.6 erg s^{-1}, its bolometric luminosity is calculated according to Flower (1996) from $m_V = 4.09$ and $B - V = 0.54$ to be $3.3 L_{bol\odot}$ and therefore its activity indicator is $L_X/L_{bol} = -6.5$, marking υ And as a rather inactive star.

If the chromospheric data really track the stellar rotation, one might expect to see variability with that period also in X-rays. This is different from the expected minima and maxima

Table 2. Spectral modeling results with 1σ errors; emission measure given in units of 10^{50} cm^{-3}.

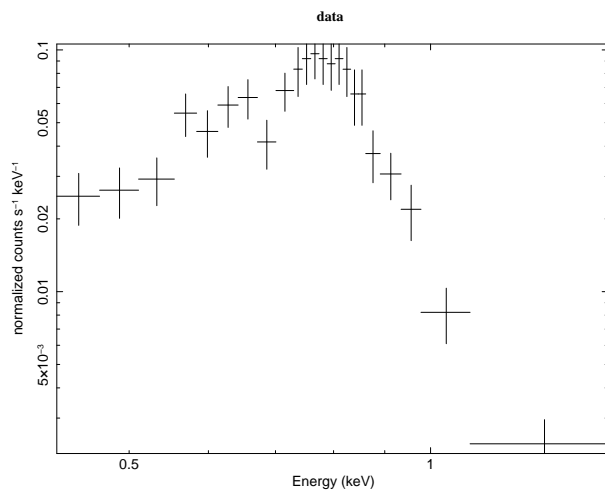| Parameter	obs. 1	obs. 2	obs. 3	obs.4	all
T_1 (MK)	2.7 ± 0.1	3.1 ± 0.1	3.0 ± 0.2	2.8 ± 0.1	2.9 ± 0.1
EM_1	8.1 ± 1.6	4.4 ± 0.7	4.1 ± 0.9	6.2 ± 1.0	5.2 ± 0.5
O	0.15 ± 0.06	0.34 ± 0.10	0.24 ± 0.09	0.16 ± 0.05	0.23 ± 0.04
Ne	0.22 ± 0.08	0.26 ± 0.10	0.25 ± 0.10	0.18 ± 0.09	0.23 ± 0.05
χ^2_{red} (d.o.f.)	0.81 (21)	0.79 (20)	0.78 (14)	1.47 (19)	1.19 (86)
expected SPI state	maximum	minimum	minimum	maximum	-
$\log L_X$ (0.25-2.0 keV)	27.80	27.62	27.56	27.69	27.65
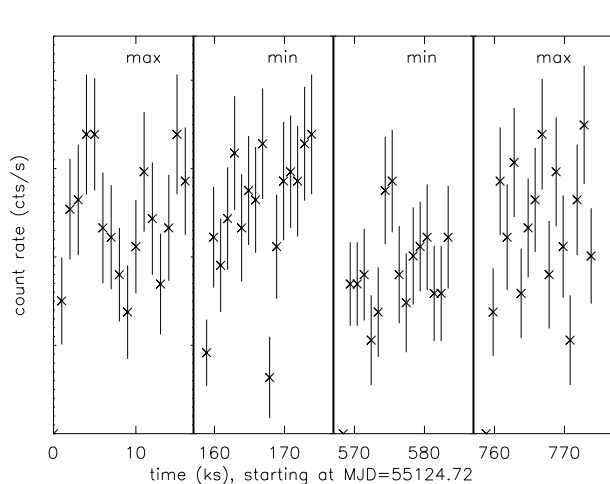
Fig. 6. Background-subtracted X-ray lightcurves of υ And, taken with *Chandra* ACIS-S in the 0.4-2.0 keV energy band, with expected SPI states according to Shkolnik et al. (2005) indicated.

Fig. 7. *Chandra* ACIS-S spectrum of υ And extracted from a single 15 ks exposure. Strong emission in the iron line complexes around 800 eV is visible.

mentioned in Table 1, since we are now dealing with the chromospheric variability from our nearly-simultaneous optical data with a period of 9.5 d. We indicated the times of the *Chandra* pointings as solid vertical lines in Fig. 4. The first, third and last observation took place at times where the chromospheric activity was (by comparison) high, while the second observation was conducted at moderate chromospheric activity. The mean count rate and mean X-ray luminosity is lower in observation three, but observation two yields comparable values to the first and last observation. We conclude that the coronal activity seems to be dominated by short-term statistical variations and not by the periodicity seen in the chromospheric data.

4. Discussion

Searching for signatures of SPI has proven to be a subtle task. Initial chromospheric measurements indicated that HD 179949's and υ And's chromospheric Ca II fluxes varied with the respective planetary period, but follow-up observations could only detect variability with the stellar rotation period. Previous attempts to observe possible SPI signatures in X-rays have been unsuccessful as well.

The υ And system was one of the prime suspects for observing SPI at work in individual star-planet systems based upon chromospheric observations (Shkolnik et al. 2005). However, our observations of the system do not show any significant variations which could be attributed to planetary effects. The variations in the chromospheric Ca II K line cores are small and are consistent with the stellar rotation period. The magnitude of the

variations is $\approx$ 0.6% of the flux in the pseudo-continuum between the Ca II H and K line. From optical and X-ray monitoring of stars such as 61 Cyg (Hempelmann et al. 2006), we know that changes in the S-index (counts in Ca II H and K lines normalized by counts in continuum stretches) of $\pm 15\%$ translate to changes in the 0.2$-$2.0 keV X-ray band of $\pm 40\%$. So, the extremely small chromospheric variations of υ And should, if ruled by the same activity effects, cause coronal variations of less than two percent over one stellar rotation period. This is much lower than the typical intrinsic variation level of a late-type star. One would only expect strong SPI signatures in X-rays here if the SPI mechanism is fundamentally different from normal activity processes, for example, if SPI happened via Jupiter-Io-like interactions where the star and its close planet are connected via flux tubes (which cannot be the case for the υ And system since the stellar rotation period is longer than the planetary orbital period). For υ And we see that the star does not show any signs of planet-induced activity; it is rather a low-activity star with some indication for rotational modulation in chromospheric emissions.

From this data and other searches for SPI signatures, it seems that stars with low to moderate activity do only exhibit very low levels of SPI effects, if at all. To unambiguously detect SPI signatures in the future, stars with extremely close-in planets (< 2 d) will be the most promising candidates. According to recent models (Lanza 2009), magnetic SPI can occur not only through reconnection between the stellar and planetary magnetic field lines, but also by the planetary field disturbing stellar magnetic loops which have stored energy by normal stellar activity processes and triggering the release of energy. Thus stars

with higher activity levels could be worthwhile targets for SPI searches if observed with good phase coverage to enable a differentiation between intrinsic stellar variability and possible SPI effects.

5. Conclusions

Our main results are summarized as follows:

1. υ And is a star of low chromospheric activity, with the coronal activity consistently being at a low level as well, indicated by the coronal activity indicator $\log L_X/L_{bol} = -6.5$.
2. Our data show variations of the Ca II K line core emission compared to the mean spectrum. These variations have a period of ≈ 9.5 d, close to the stellar rotation period of ≈ 8.5 d.
3. The X-ray data do not show significant changes between expected SPI maximum and minimum states, neither in the lightcurves nor in the spectra. The spectra show a FIP effect, with iron being overabundant by a factor of ≈ 4 compared to neon, typical for stars with low to moderate X-ray activity.
4. In our observations, the υ And system does not show signatures of Star-Planet-Interactions. The periodicity observed in chromospheric activity indicators is very close to the calculated stellar rotation period and is therefore probably induced by non-SPI-related active regions on the star. Observational evidence for Star-Planet-Interactions in X-rays remains elusive.

References

Cuntz, M., Saar, S. H., & Musielak, Z. E. 2000, ApJ, 533, L151
Erkaev, N. V., Kulikov, Y. N., Lammer, H., et al. 2007, A&A, 472, 329
Flower, P. J. 1996, ApJ, 469, 355
Gilliland, R. L. & Baliunas, S. L. 1987, ApJ, 314, 766
Goldreich, P. & Lynden-Bell, D. 1969, ApJ, 156, 59
Gonzalez, G., Carlson, M. K., & Tobin, R. W. 2010, MNRAS, 403, 1368
Grevesse, N. & Sauval, A. J. 1998, Space Science Reviews, 85, 161
Hall, J. C., Lockwood, G. W., & Skiff, B. A. 2007, AJ, 133, 862
Hempelmann, A., Robrade, J., Schmitt, J. H. M. M., et al. 2006, A&A, 460, 261
Henry, G. W., Baliunas, S. L., Donahue, R. A., Fekel, F. C., & Soon, W. 2000, ApJ, 531, 415
Kashyap, V. L., Drake, J. J., & Saar, S. H. 2008, ApJ, 687, 1339
Lammer, H., Selsis, F., Ribas, I., et al. 2003, ApJ, 598, L121
Lanza, A. F. 2008, A&A, 487, 1163
Lanza, A. F. 2009, A&A, 505, 339
Lecavelier Des Etangs, A. 2007, A&A, 461, 1185
Lomb, N. R. 1976, Ap&SS, 39, 447
Poppenhaeger, K., Robrade, J., & Schmitt, J. H. M. M. 2010, A&A, 515, A98+
Scargle, J. D. 1982, ApJ, 263, 835
Scharf, C. A. 2010, ApJ, 722, 1547
Schmitt, J. H. M. M. 2009, in American Institute of Physics Conference Series, Vol. 1094, American Institute of Physics Conference Series, ed. E. Stempels, 473–476
Shkolnik, E., Bohlender, D. A., Walker, G. A. H., & Collier Cameron, A. 2008, ApJ, 676, 628
Shkolnik, E., Walker, G. A. H., Bohlender, D. A., Gu, P., & Kürster, M. 2005, ApJ, 622, 1075